Alma Mater Studiorum Università di Bologna
Archivio istituzionale della ricerca

Photophysical Properties of 4-Dicyanomethylene-2-methyl-6-(p-dimethylamino-styryl)-4H-pyran Revisited: Fluorescence versus Photoisomerization

(Article begins on next page)

20 April 2024

Photophysical Properties of 4-Dicyanomethylene-2-methyl-6-(p-dimethylamino-styryl)-4H-pyran Revisited: Fluorescence versus Photoisomerization

Lorenzo Casimiro+,[a, b, c] Stéphane Maisonneuve+,[a] Pascal Retailleau,[d] Serena Silvi,[b, c] Juan Xie,*[a] and Rémi Métivier*[a]

[a] Dr. L. Casimiro,+ Dr. S. Maisonneuve,+ Prof. J. Xie, Dr. R. Métivier
ENS Paris-Saclay, CNRS, PPSM
Université Paris-Saclay, 91190 Gif-sur-Yvette (France)
E-mail: joanne.xie@ens-paris-saclay.fr
remi.metivier@ens-paris-saclay.fr
[b] Dr. L. Casimiro,+ Dr. S. Silvi
CLAN-Center for Light Activated Nanostructures
Università di Bologna and Consiglio Nazionale delle Ricerche
Via Gobetti 101, 40129 Bologna (Italy)
[c] Dr. L. Casimiro,+ Dr. S. Silvi
Dipartimento di Chimica "G. Ciamician", Università di Bologna
Via Selmi 2, 40126 Bologna (Italy)
[d] Dr. P. Retailleau
ICSN, CNRS UPR 2301, Universit8 Paris-Saclay, Gif-Sur-Yvette 91198 (France)
[+] These authors contributed equally to this work.

Abstract

Although 4-dicyanomethylene-2-methyl-6-(*p*-dimethylamino-styryl)-4*H*-pyran (DCM) has been known for many decades as a bright and photostable fluorophore, used for a wide variety of applications in chemistry, biology and physics, only little attention has been paid so far to the presence of multiple isomers and conformers, namely *s-trans*-(*E*), *s-cis*-(*E*), *s-trans*-(*Z*), and *s-cis*-(*Z*). In particular, light-induced *E–Z* isomerization plays a great role on the overall photophysical properties of DCM. Herein, we give a full description of a photoswitchable DCM derivative by a combination of structural, theoretical and spectroscopic methods. The main *s-trans*-(*E*) isomer is responsible for most of the fluorescence features, whereas the *s-cis*-(*E*) conformer only contributes marginally. The non-emitting *Z* isomers are generated in large conversion yields upon illumination with visible light (e.g., 485 or 514 nm) and converted back to the *E* forms by UV irradiation (e.g., 365 nm). Such photoswitching is efficient and reversible, with high fatigue resistance. The *E→Z* and *Z→E* photoisomerization quantum yields were determined in different solvents and at different irradiation wavelengths. Interestingly, the fluorescence and photoisomerization properties are strongly influenced by the solvent polarity: the fluorescence is predominant at higher polarity, whereas photoisomerization becomes more efficient at lower polarity. Intermediate medium (THF) represents an optimized situation with a good balance between these two features.

Introduction

The continuous growth in the field of photoactive molecules, gradually coupled in the last decades with advances in functional nanoscaled materials, has led to a wide range of applications, particularly in the field of optoelectronics, molecular nanoprobes, photo-responsive multifunctional devices, or super-resolution imaging.[1] For these purposes, a better understanding of fluorescent molecular components, aimed at fulfilling specific optical or biological applications, is of pivotal importance. In such a context, 4-dicyanomethylene-2-methyl-6-(*p*-dimethylaminostyryl)-4*H*-pyran (DCM, Figure 1) provides an excellent prototype. DCM is a well-known fluorophore with strong red emission.[2] Moreover, its charge-transfer character from the electron-donating amine to the electron-withdrawing dicyanomethylene-pyranyl moiety confers strong solvatochromism to this dye, with the possibility of tuning the absorption and emission by means of solvent polarity. For all these reasons, DCM has found many applications in laser dyes,[2, 3] chemo- or biosensors,[4] in dopants or hosts for OLEDs,[5] in nonlinear optics materials,[6] or in supramolecular photoactive architectures[7] and logic gates.[8] In the last decades, the solvatochromism of DCM has been extensively investigated by steady-state spectroscopy[3b, 9] as well as time-resolved techniques,[10] showing the strong photoinduced intramolecular charge-transfer nature of its emissive excited state, which has been confirmed by theoretical studies.[11] The photophysics of DCM has been mostly detailed in solution, but also in a variety of organized media (microemulsions, vesicles, micelles, and aggregates).[12] Interestingly, due to the presence of an ethylenic central bond, DCM can in principle undergo *E–Z* photoisomerization, that is, behave as a photochromic compound. This photoswitching ability would be extremely appealing, as it would not only influence its fluorescence properties, but also disclose new routes for fine tuning the optical properties of the

fluorophore. However, among the very large number of examples involving DCM in the literature, only a limited number of qualitative studies have been reported on this phenomenon.[10a, 11b, 13] Moreover, aspects related to the complete conformational isomerism have never been deeply elucidated in experimental studies reported so far, and the conformation has been randomly presented in most reported structures.
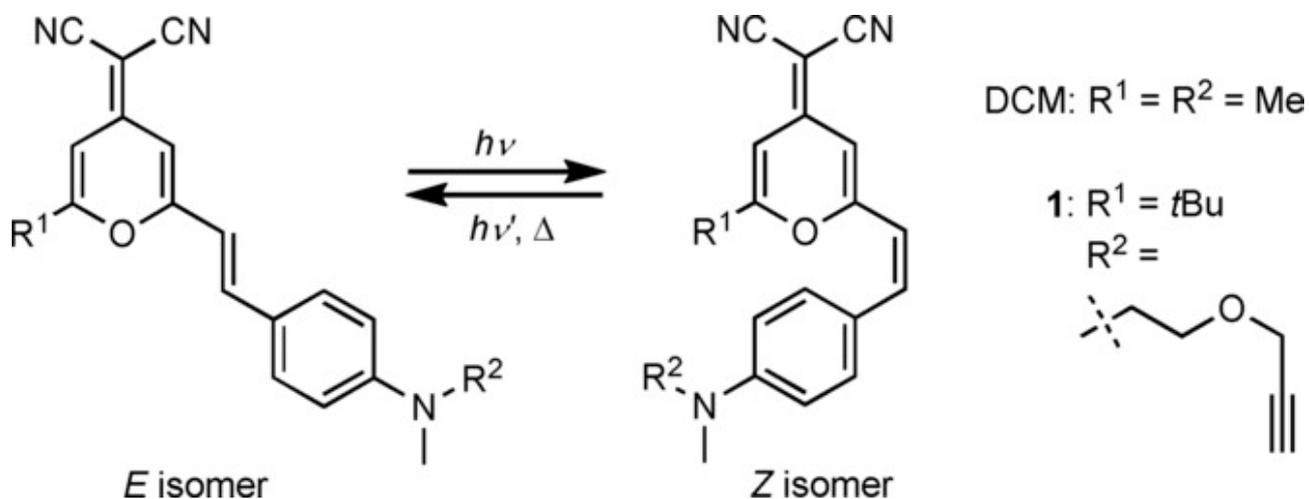

Figure 1. Structure and *E–Z* photoisomerization reaction of commercial DCM and compound **1**.

In this context, we decided to fully rationalize and quantify the fluorescence and photo-induced isomerization of a DCM derivative, **1**, bearing a propargylic unit on the aniline function for further functionalization. Therefore, we report herewith its complete structural and photophysical characterization by means of X-ray diffraction (XRD), DFT calculations, steady-state and time-resolved spectroscopy, with a particular emphasis on the solvent effect. It appears that the DCM derivative **1** behaves as an efficient fluorescent-photochromic molecule, with an interesting combination of properties for photoswitching purposes: 1) the emission of the *E* isomer is bright and tunable by the solvent polarity, 2) the *Z* isomer is not emissive, and 3) the *E–Z* photoisomerization efficiency is wavelength dependent and strongly affected by the polarity of the medium.

Results

Synthesis, structure characterization and isomers identification

Compound (*E*)-**1** was synthesized according to previously reported procedures[14] with special care to avoid any exposure to UV–visible light during the synthesis, yielding a red crystalline powder.

After recrystallization in MeCN and filtration, single monocrystals were isolated and XRD

experiment was performed. Compound (*E*)-**1** crystallizes in the triclinic space group ($P\bar{1}$) with layers of coplanar molecules oriented in the same direction and arranged head-to-tail between adjacent layers, as depicted in Figure S1 in the Supporting Information. Its molecular structure shows clearly the *s-trans*-(*E*) configuration of **1**, according to the positions of the two double bonds

(Figure 2, Table S1). *s-trans-*(*E*)-**1** is almost entirely planar, including the dicyanomethylene substituent, with less than 5° between the planes of the two cyclic units. The central C=C bond is equal to 1.336 Å, which confirms its π character. The two C−C bonds on both sides of this central double bond, equal to 1.426 and 1.444 Å, are shorter than the values theoretically expected for single bonds, demonstrating the conjugated character of the main body of the molecule. In addition, the C≡CH and C≡N bonds are measured at 1.136 Å and on average 1.146 Å respectively, corresponding well to triple bonds.
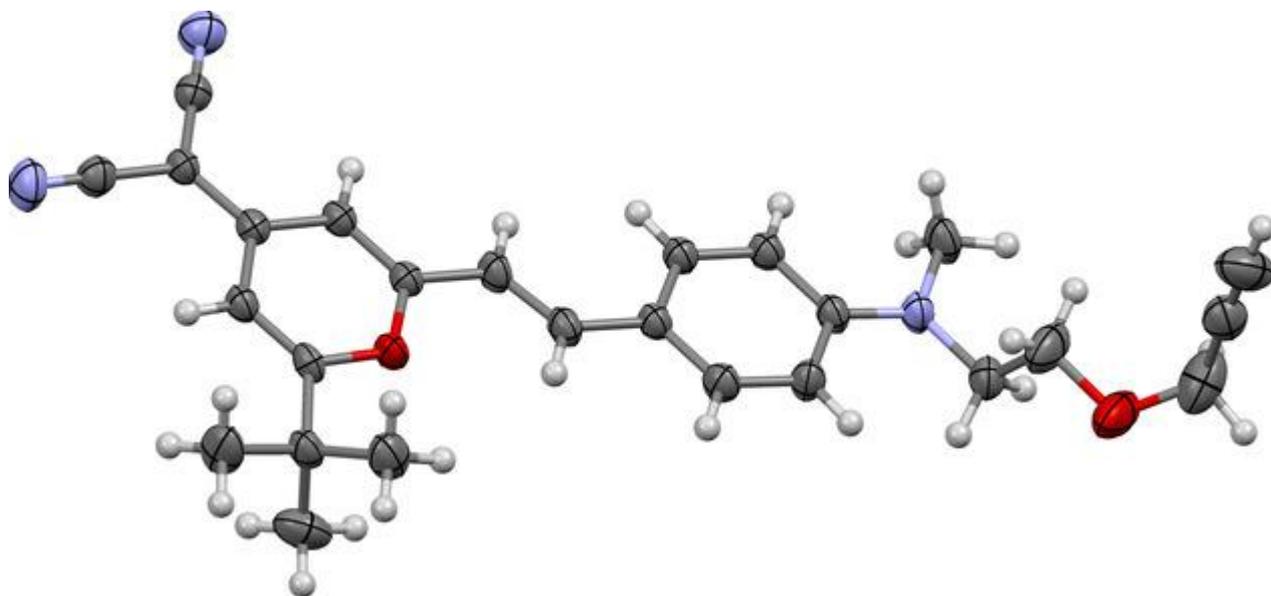

Figure 2. X-ray diffraction structure of compound **1** in the *s-trans-*(*E*) form, represented with thermal ellipsoids at the 25 % probability level.

Theoretical calculations were carried out to identify the different geometries, energies and dipole moments of the accessible isomeric states of **1** in solution. Indeed, in addition to the two configurational isomers, that is, *E* and *Z*, **1** can in principle exist in two conformers, obtained by rotation around the single bond in position 6 on the pyranyl moiety. Thus, depending on the reciprocal position of the two C=C double bonds, four isomers, namely *s-trans-*(*E*), *s-cis-*(*E*), *s-trans-*(*Z*), *s-cis-*(*Z*), can be defined (Figure 3, insets).[11b] This variety of geometrical structures is of great importance, as it can be assumed that each particular isomer possesses peculiar features and contributes in a different way to the overall properties of **1** in solution. DFT computations were performed with the PBE0 functional and the 6–311+G(d,p) basis set in vacuum. The geometry optimization provided the conformation, ground-state energies and the dipolar moments of the four isomers/conformers identified: *s-trans-*(*E*)-**1**, *s-cis-*(*E*)-**1**, *s-trans-*(*Z*)-**1**, and *s-cis-*(*Z*)-**1** (Figure 3). As expected, the *s-trans-*(*E*)-**1** is the most stable form, whereas the *s-cis-*(*E*)-**1** is only 1.9 kcal mol^{-1} less stable than the former. Based on these relative energies, both conformers are populated at room temperature, the Boltzmann distribution provides a thermal population of *s-trans-*(*E*)-**1** : *s-cis-*(*E*)-**1** around 96:4. On the contrary, both *Z* isomers are much higher in energy: the *s-cis-*(*Z*)-**1** isomer resulted to be 6.4 kcal mol^{-1} higher than the *s-trans-*(*E*)-**1**, and slightly more stable (by ~1.2 kcal mol^{-1}) than the *s-trans-*(*Z*)-**1**. Consequently, the *Z* isomers cannot be obtained spontaneously at

room temperature from the initial *E* form, unless being appropriately activated by a photoinduced isomerization (Figure 1), and should reach a Boltzmann distribution of *s-cis*-(*Z*)-**1** : *s-trans*-(*Z*)-**1** around 89:11. The electrical dipole moments obtained by DFT are comparable between the two *E* isomers (19 D) and the *s-trans*-(*Z*)-**1** (17 D), while that of the *s-cis*-(*Z*)-**1** is much lower (12 D), since in this form the compound adopts a strongly folded geometry (Figure 3).
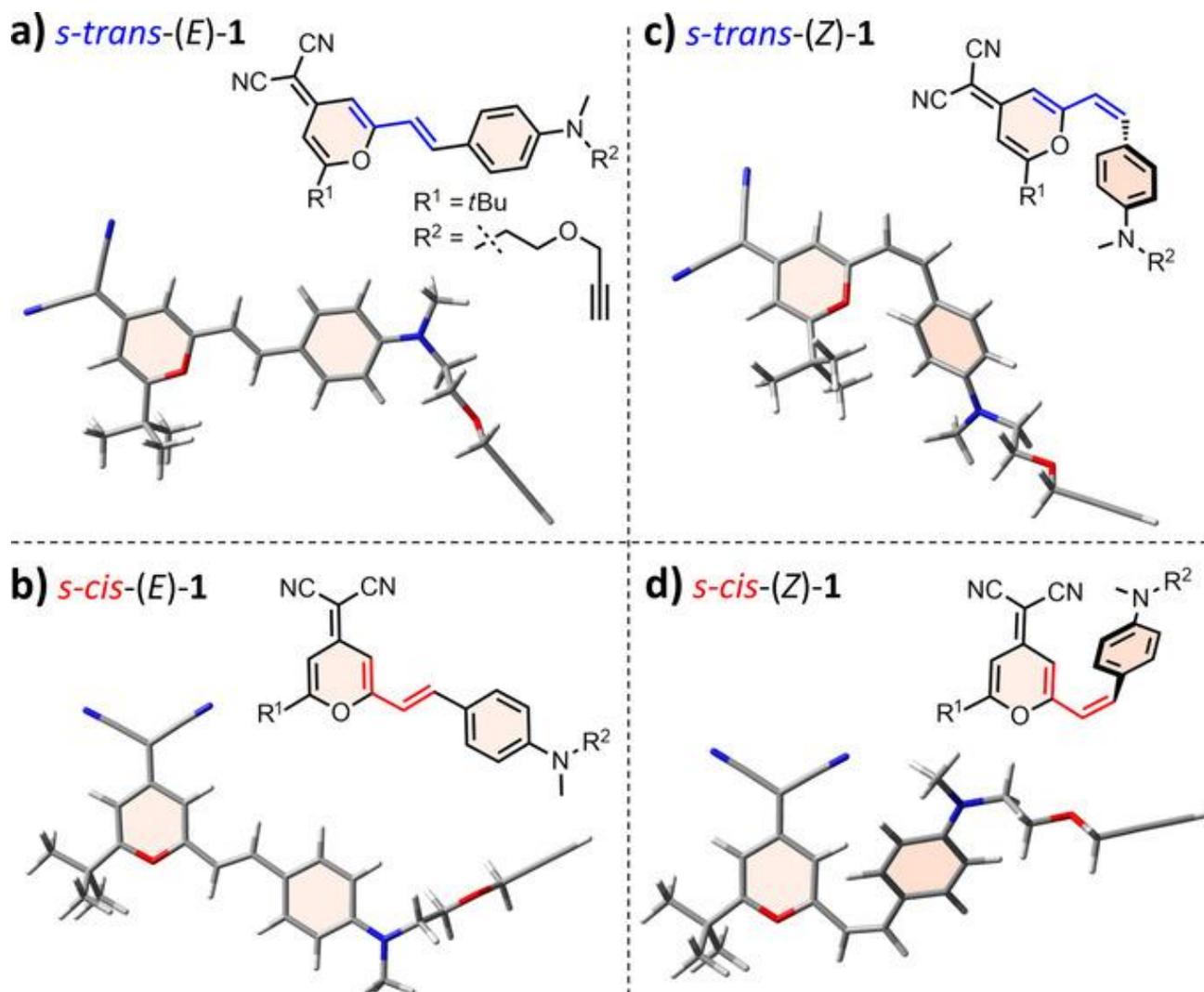
Figure 3. Optimized geometries of the four isomers/conformers identified for **1**, calculated by DFT PBE0/6–311+G(d,p) in a vacuum: a, b) *E* isomers, c, d) *Z* isomers; a, c) *s-trans* conformers (blue bonds), b, d) *s-cis* conformers (red bonds). Insets: corresponding chemical structure.

Steady-state and time-resolved spectroscopy

The absorption and fluorescence spectra of (*E*)-**1** were recorded in cyclohexane, toluene (PhMe), chloroform, ethyl acetate, tetrahydrofuran (THF), dichloromethane, ethanol and acetonitrile (MeCN), spanning a wide range of polarity levels (Figure S4). Three representative solvents have been selected in the following work: PhMe (lower polarity), THF (medium polarity) and MeCN

(higher polarity). The absorption spectra displayed in Figure 4 show the typical features of DCM derivatives[2] with an intense absorption band centered in the visible region as well as a weak and structured band located in the medium UV range. As the polarity decreases, the main band is only slightly affected, with maxima at 465, 467 and 463 nm in MeCN, THF and PhMe, respectively, and the vibrational structure becomes gradually more pronounced. The molar absorption coefficient turned out to be rather insensitive to the solvent and the values are between 53 900 L mol^{-1} cm^{-1} in MeCN and 47 700 L mol^{-1} cm^{-1} in PhMe (Table 1). As previously reported for DCM-based derivatives, compound (E)-**1** was found to exhibit a marked fluorescence solvatochromism:[3b, 9] the emission band is strongly blue-shifted as the polarity decreases, and the maximum wavelength moves from 620 nm in MeCN to 548 nm in PhMe, resulting in a shortening of the Stokes shift from 5400 cm^{-1} in MeCN to 3400 cm^{-1} in PhMe (Table 1). The complete set of data as a function of the solvent polarity was used to plot the Lippert–Mataga graph shown in Figure S4, providing an enhancement of the dipolar moment between the ground and excited state $\Delta\mu$ as high as 14.4 D. In a similar manner, the emission quantum yield Φ_{em} is affected by the solvent polarity, from 0.55 in MeCN down to 0.02 in PhMe (Table 1), which is consistent with previous studies on DCM.[9b]
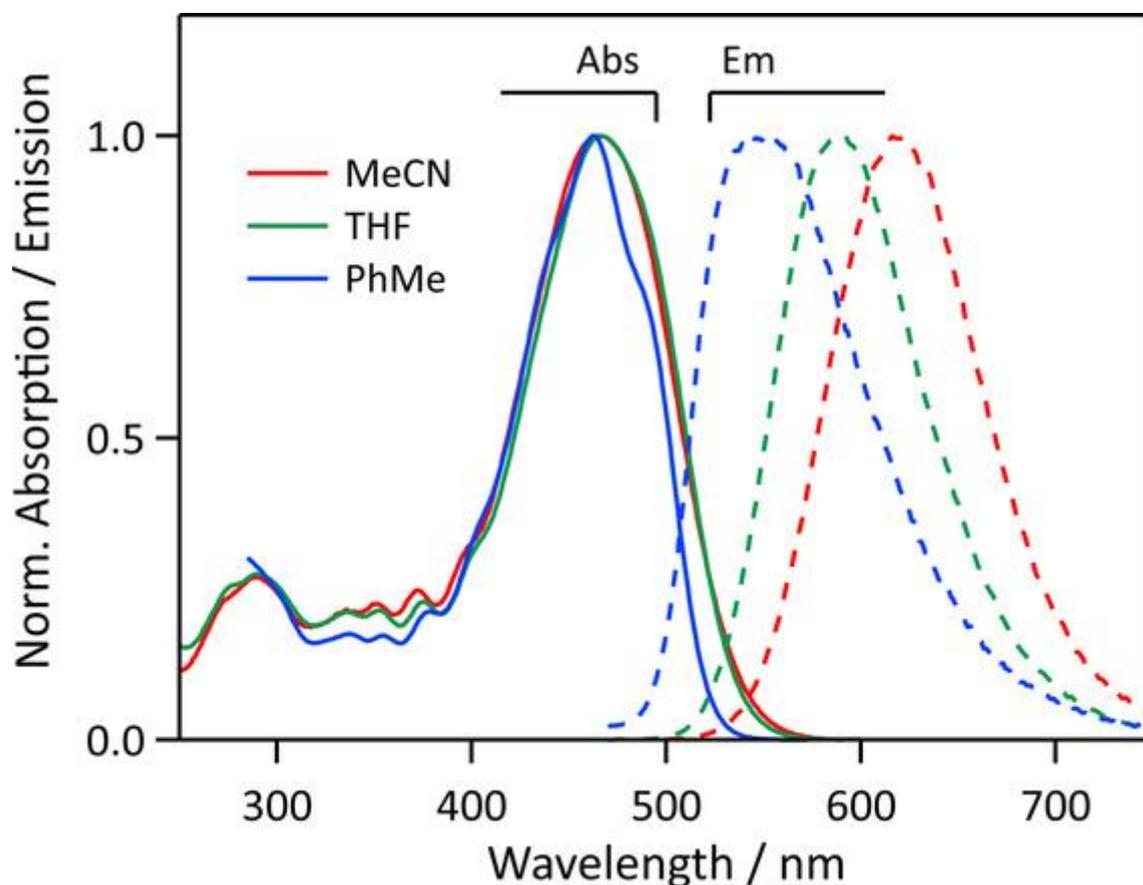

Figure 4. Absorption (solid lines) and emission (dashed lines) spectra of (E)-**1** in MeCN, THF, and PhMe. λ_{ex}=392 nm.

Table 1. Steady-state absorption and emission properties of (E)-**1** determined in MeCN, THF and PhMe.

	λ_{abs}	ϵ	λ_{em}	Φ_{em}[a]	Stokes shift
	[nm]	[L mol^{-1} cm^{-1}]	[nm]		[cm^{-1}]
MeCN	465	53 900	620	0.55	5 400
THF	467	49 600	590	0.32	4 400
PhMe	463	47 700	548	0.02	3 400

[a] Average values obtained by excitation in the visible region.

Fluorescence decay curves were recorded by the time-correlated single-photon counting (TCSPC) technique in MeCN, THF and PhMe, as shown in Figure 5. The emission decays collected at three different emission wavelengths for each solvent have been fitted by a global analysis procedure using a bi-exponential function.[13c, 13d, 15] All fits were satisfactory ($\chi_R^2 < 1.2$) and provided a pre-exponential factor $a_1 > 0.79$ for the main time constant τ_1, and a minor contribution ($a_2 < 0.21$) for the short component τ_2 (Table 2) The major component τ_1 was found to drastically decrease when the solvent polarity decreases, from MeCN (2.31±0.01 ns) to THF (1.25±0.01 ns) and PhMe (0.14±0.01 ns). The second minor component τ_2 was determined to be 0.43±0.04 ns in MeCN and 0.22±0.02 ns in THF. The value of $\tau_2 < 10$ ps in PhMe is even shorter than our instrumental resolution limit. Interestingly, the contribution of τ_2 is appreciable at short emission wavelengths (0.16 in MeCN, 0.14 in THF, 0.21 in PhMe) but drops to very low values at longer emission wavelengths (0.08 in MeCN and THF, negligible in PhMe), showing that this component arises mostly from the blue edge of the fluorescence spectrum (Table 2). Given the values of the decay time-constants τ_i and the pre-exponential factors a_i, the normalized fractions of intensity f_i were calculated (Table 2): in all solvents and whatever the emission wavelength, the major component τ_1 counts for more than 97 % of the collected emission. Moreover, the influence of light irradiation on the emission decays has been examined. The fluorescence decay curves were recorded before and after irradiation at 514 nm, and no noticeable change could be detected, as shown in Table 2.
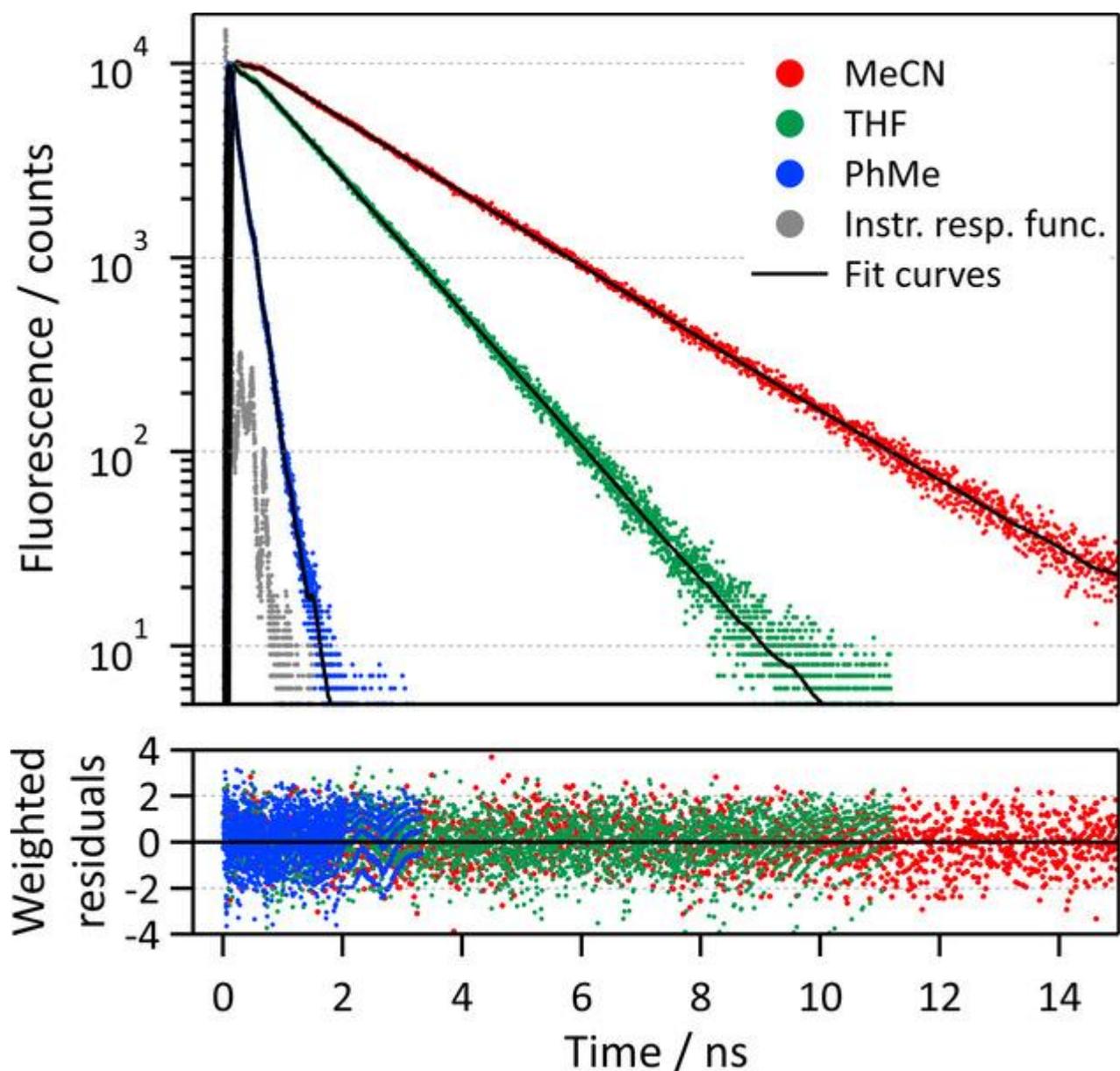
Figure 5. Fluorescence decay curves, instrumental response function, multiexponential fitting, and weighted residuals of (*E*)-**1** in MeCN, THF, and PhMe. λ_{ex}=400 nm; λ_{em}=620 (MeCN), 590 (THF), or 550 nm (PhMe).

Table 2. Time-resolved fluorescence parameters of (*E*)-**1** determined in MeCN, THF and PhMe.[a]

	λ_{em} [nm]	τ_1 [ns]	a_1 (f_1)[d]	τ_2 [ns]	a_2 (f_2)[d]
MeCN	580	2.31±0.01	0.84 (0.97)	0.43±0.04	0.16 (0.03)
	620	2.31±0.01	0.89 (0.98)	0.43±0.04	0.11 (0.02)
	660	2.31±0.01	0.92 (0.98)	0.43±0.04	0.08 (0.02)
	620 (irr)[b]	2.31±0.01	0.89 (0.98)	0.43±0.04	0.11 (0.02)
THF	550	1.25±0.01	0.86 (0.97)	0.22±0.02	0.14 (0.03)
	590	1.25±0.01	0.90 (0.98)	0.22±0.02	0.10 (0.02)

	λ_{em} [nm]	τ_1 [ns]	a_1 (f_1)[d]	τ_2 [ns]	a_2 (f_2)[d]
	650	1.25±0.01	0.93 (0.99)	0.22±0.02	0.08 (0.01)
	590 (irr)[b]	1.25±0.01	0.90 (0.98)	0.23±0.02	0.10 (0.02)
PhMe	500[c]	0.14±0.01	0.79 (0.97)	<0.01	0.21 (0.02)
	550	0.14±0.01	1.00 (1.00)	–	–
	590	0.14±0.01	1.00 (1.00)	–	–
	550 (irr)[b]	0.14±0.01	1.00 (1.00)	–	–

[a] Excitation wavelength λ_{ex}=400 nm. [b] After irradiation at λ_{irr}=514 nm. [c] An additional time-constant of 1.6±0.1 ns was necessary to obtain satisfactory fit for this particular decay, with negligible pre-exponential coefficient (<0.01). [d] a_i: pre-exponential factors; f_i: fractions of intensity with $f_i=a_i\times\tau_i/\Sigma(a_j\times\tau_j)$.

Photoisomerization properties

Light-induced photoreactions of compound **1** were investigated in deaerated MeCN, THF and PhMe. Irradiation in the UV–visible range induced, in all the three solvents, appreciable variations of the absorption spectra, namely a decrease of the main visible band and the uprising of the band comprised in the 300–400 nm range (Figure 6 a). The isosbestic point observed around 394 nm suggests a transformation between two main species. These spectral changes are consistent with a photoinduced isomerization, from the most stable (*E*)-**1** form to the metastable (*Z*)-**1** form, as shown by ^{1}H NMR (Figure S3) and preliminarily reported in previous works.[10a, 13b, 13c, 13e] A prolonged illumination at different wavelengths leads to photostationary states (PSS) associated with different maximum ratios *Z*:*E*. As depicted in Figure 6 a, irradiation in the blue region of the visible spectrum (485 and 514 nm) induces a large variation of absorption, whereas UV or violet irradiation (365, 405 nm) leads to moderate absorption changes. After illumination, the samples were kept in the dark. Because the *E* isomer is expected to be thermodynamically more stable than the *Z* form (vide supra), a *Z*→*E* isomerization could be expected. However, no appreciable variation of the absorbance was detected over a long period of time (one day), thus suggesting that the thermal *Z*→*E* back-reaction is extremely slow, with half-life values $t_{1/2}$ estimated to be higher than ∼15 days in all solvents, as shown in Figure S6–S8.
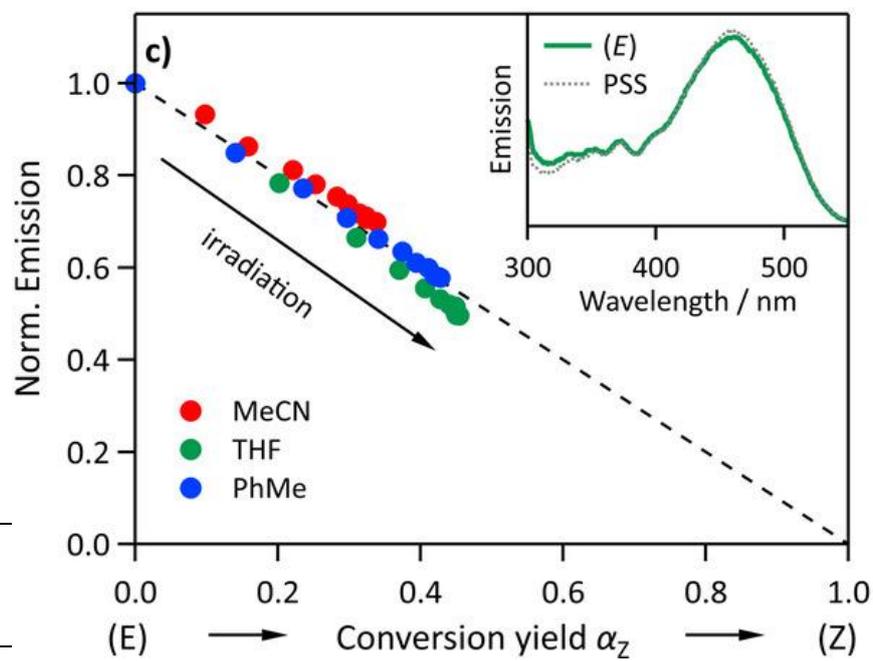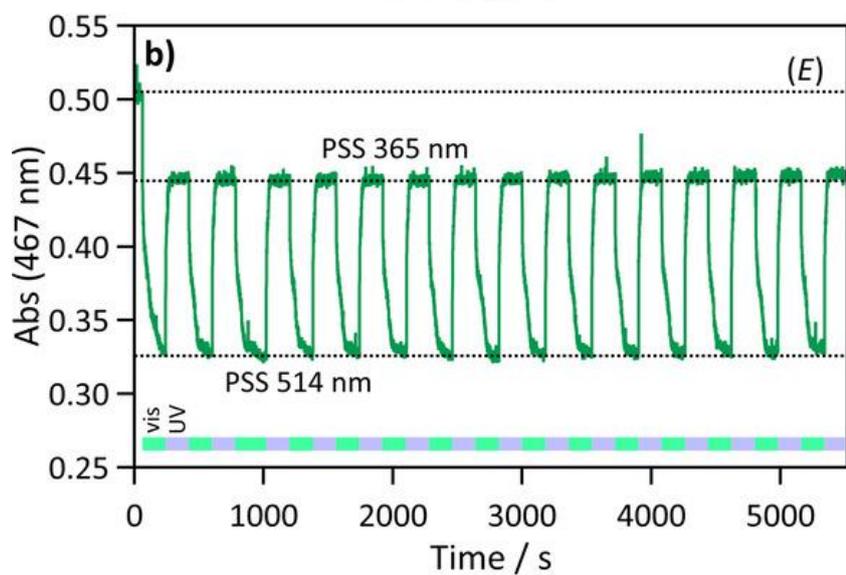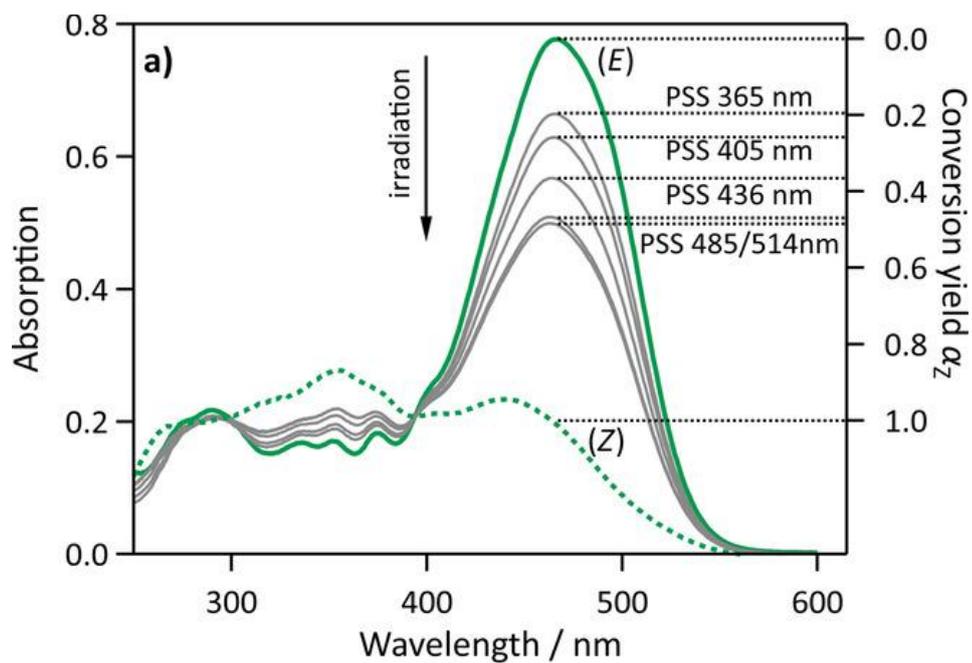
a)

b)

c)

Figure 6. a) Absorption spectra of **1** in THF as the *E* isomer before irradiation (green curve), at the photostationary state under prolonged irradiation at 365, 405, 436, 485, and 514 nm (PSS, gray curves) and of (*Z*)-**1** as extrapolated from HPLC experiments [green dotted curve, see Eq. (1)]. b) Absorbance at 467 nm of **1** in THF as function of time, during 15 cycles of visible (514 nm, 13.7 mW, 3 min) and UV (365 nm, 3.9 mW, 3 min) irradiation showing efficient and reversible photoswitching between the PSS at 514 nm and the PSS at 365 nm. c) Correlation plot between the normalized emission intensity and the degree of *E*–*Z* photoconversion in MeCN, THF, and PhMe under irradiation at 514 nm. Inset: excitation spectra (λ_{em}=600 nm) of **1** as the *E* isomer before irradiation (green curve) and at the PSS at 514 nm (gray dotted curve).

PSS are characterized by their associated conversion yields α_Z, i.e., the fraction of *Z* form obtained under irradiation at a given λ_{irr}. Thanks to the difference in polarity and the good thermal stability of both *E* and *Z* isomers, the exact compositions of the PSS (α_Z) were quantified by HPLC (Figure S2). Following, the absorption spectra of (*Z*)-**1** isomer in the three solvents were obtained from the corresponding spectra of the *E* isomer and the PSS according to Equation 1:

$$(1) \quad A_Z(\lambda) = A_E(\lambda) + \frac{A_{PSS}(\lambda) - A_E(\lambda)}{\alpha_Z}$$

The absorption spectrum of (*Z*)-**1** in THF is displayed in Figure 6 a, as well as the α_Z scale: the highest *E*→*Z* photoconversion extent was obtained at 485 and 514 nm (α_Z=0.45).

The fatigue resistance of **1** was then evaluated in MeCN, THF and PhMe with 15 cycles of alternate irradiations at 514 and 365 nm. The absorption profiles showed in Figure S5 demonstrate that the system can be switched between two different states (PSS 514 and PSS 365 nm), in a reversible manner and without any noticeable degradation after 15 cycles. More accurate investigation of the reversible photoswitching is displayed in Figure 6 b: the absorbance recorded at 467 nm corresponds initially to the (*E*)-**1** form, then switches between two PSS levels under illumination sequences at 514 and 365 nm. The reversibility of the molecule is fully achieved with fast rates under these experimental conditions: 1 min of irradiation at 514 nm (13.7 mW) is required to reach the corresponding PSS, and 15 s of irradiation at 365 nm (3.9 mW) is enough to reach more than 80 % of the transformation between the PSS 514 nm and PSS 365 nm (Figure 6 b).

Besides absorption, the fluorescence properties of (*E*)-**1** were found to be affected by light stimulation. The emission spectral shapes are not modified upon irradiation, but the emission intensity decreases along with the light exposure, which indicates that the (*Z*)-**1** isomer is less emissive than the (*E*)-**1** (Figure S9). To investigate more quantitatively the fluorescence photoswitching properties of **1**, a correlation between the emission intensity and the degree of photoconversion α_Z was performed (Figure 6 c). In all the three solvents, the correlation plot shows a clear linear decreasing relationship, for which the extent of fluorescence quenching reflects the conversion yield α_Z. Extrapolation of the data suggests that there is no more emission at total conversion. Moreover, the excitation spectra of the pure (*E*)-**1** form and the PSS at 514 nm are superimposable (Figure 6 c, inset), which means that the emission is due to the sole *E* isomer. A series of UV–visible irradiation sequences was also performed, without significant changes in the fluorescence levels of the two states after 15 consecutive cycles (Figure S10), confirming the excellent reversible fluorescence photoswitching properties of **1**.

Photokinetic experiments of compound **1** under different irradiation wavelengths were carried out in MeCN, THF and PhMe, in order to quantify accurately the $E{\to}Z$ and $Z{\to}E$ photoisomerization reactions (Figure 7). As the thermal back reaction was found to be very slow in all solvents, it was considered negligible in the time-scale of the photokinetic measurements. The overall differential photokinetic equation related to the E–Z light-induced interconversion can be written [Eq. 2]:[16]

$$(2) \qquad \frac{\mathrm{d}C_Z}{\mathrm{d}t} = -\frac{\mathrm{d}C_E}{\mathrm{d}t} = \Phi_{EZ} \times I_E^{\mathrm{abs}}(\lambda_{\mathrm{irr}}, t) - \Phi_{ZE} \times I_Z^{\mathrm{abs}}(\lambda_{\mathrm{irr}}, t)$$
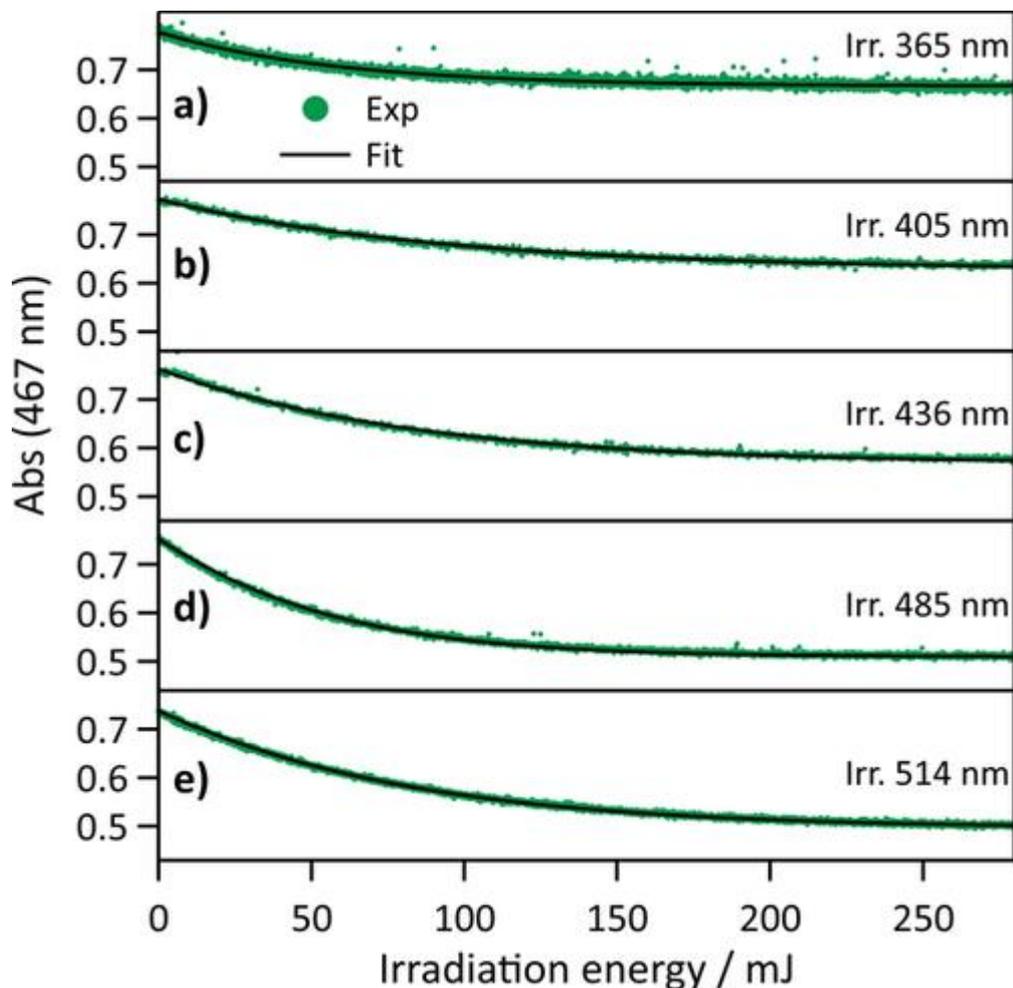
Figure 7. Absorbance at 467 nm of **1** in THF as a function of cumulated irradiation energy at a) 365, b) 405, c) 436, d) 485, and e) 514 nm (green dots), and numerical fitting curves (black solid lines) by means of the photokinetic differential equations expressed in Equations (2)–(4). Experimental conditions: concentration=$1.55{\times}10^{-5}$ mol L^{-1}; volume=2 mL; irradiation power=112 (at 365), 380 (405), 430 (436), 207 (485), and 142 µW (at 514 nm); irradiation time=42 (at 365), 12 (405), 11 (436), 23 (485), and 33 min (at 514 nm).

where Φ_{EZ} is the quantum yield for the $E{\to}Z$ isomerization, Φ_{ZE} is the quantum yield for the $Z{\to}E$ isomerization and I^{abs} is the time-dependent intensity absorbed by the compound at the irradiation wavelength λ_{irr}, as expressed by Eqs. 3 and 4:

$$(3) \quad I_E^{abs}(\lambda_{irr}, t) = \left[\frac{1 - 10^{-Abs(\lambda_{irr}, t)}}{Abs(\lambda_{irr}, t)} \right] \times I_0(\lambda_{irr}) \, \varepsilon_E(\lambda_{irr}) \, \ell C_E(t)$$

$$(4) \quad I_Z^{abs}(\lambda_{irr}, t) = \left[\frac{1 - 10^{-Abs(\lambda_{irr}, t)}}{Abs(\lambda_{irr}, t)} \right] \times I_0(\lambda_{irr}) \, \varepsilon_Z(\lambda_{irr}) \, \ell C_Z(t)$$

with $Abs(\lambda_{irr}, t)$ the absorbance value at the irradiation wavelength during the time of the experiment and I_0 the incident irradiation intensity. A numerical iterative fitting algorithm based on Equations (2)–(4) provides the values of Φ_{EZ} and Φ_{ZE}, in all solvents and at the different irradiation wavelengths investigated. The whole set of photoisomerization quantum yields values are gathered in Table S3. Figure 8 overlays the (*E*)-**1** and (*Z*)-**1** absorption spectra, together with the Φ_{EZ}, Φ_{ZE} and α_Z values for the three solvents. As an average, the quantum yield for the $Z{\rightarrow}E$ photoisomerization (Φ_{ZE}) is ~5 times higher than that of the $E{\rightarrow}Z$ reaction (Φ_{EZ}). Such quantum yield orders of magnitude are usually observed for *E–Z* isomerization of similar photochromes, such as stilbene[17] (Φ_{EZ}=0.2–0.6, Φ_{ZE}=0.3–0.5) or azobenzene derivatives[18] (Φ_{EZ}=0.1–0.5, Φ_{ZE}=0.2–0.6). Moreover, for a given solvent, it can be noticed that the Φ_{EZ} is weakly dependent on the irradiation wavelength, whereas the value of Φ_{ZE} showed a strong wavelength dependence, with a noticeable increase when irradiation in the red edge of the absorption spectrum was employed. Besides, the solvent plays a key role in the photoisomerization reactivity of **1**.[10a, 13b, 13c, 13e] On the one hand, the Φ_{EZ} quantum yield is significantly improved in THF and PhMe (0.09 to 0.18) with respect to MeCN (0.05 to 0.07). On the other hand, the backward Φ_{ZE} quantum yield is much lower in THF (0.20 to 0.43) compared to MeCN and PhMe (up to 0.70 in PhMe). These photoisomerization quantum yields Φ_{EZ} and Φ_{ZE}, together with the respective absorption coefficients $\epsilon_E(\lambda_{irr})$ and $\epsilon_Z(\lambda_{irr})$ of the (*E*)-**1** and (*Z*)-**1** forms, define the photoconversion yield α_Z shown in the following relationship, considering both isomers as thermally stable [Eq. 5]:

$$(5) \quad \alpha_Z(\lambda_{irr}) = \frac{\varepsilon_E(\lambda_{irr}) \times \Phi_{EZ}(\lambda_{irr})}{\varepsilon_E(\lambda_{irr}) \times \Phi_{EZ}(\lambda_{irr}) + \varepsilon_Z(\lambda_{irr}) \times \Phi_{ZE}(\lambda_{irr})}$$

Figure 8. a–c) Absorption spectra of the *E* (solid lines) and *Z* (dashed lines) isomers of **1** and photoisomerization quantum yields Φ_{EZ} (full circles) and Φ_{ZE} (empty squares). d–f) Conversion yield α_Z reached at the PSS for different irradiation wavelengths. Solvents: a, d) MeCN, b, e) THF, c, f) PhMe.

The calculated values of α_Z for MeCN, THF and PhMe solvents in Figure 8 d–f are perfectly in line with the expected trends based on Equation (5) and Φ_{EZ}/ Φ_{ZE} numbers: the highest conversion yields α_Z are obtained in THF (large Φ_{EZ} but low Φ_{ZE}) compared to MeCN and PhMe. The largest fractions of (*Z*)-**1** isomer were obtained with irradiation wavelengths on the red side of the absorption bands (485 and 514 nm), for which α_Z was found to be >0.40 for the three solvents.

Discussion

The general behavior of the DCM derivative **1**, involving fluorescence but also photoisomerization processes, can be rationalized by considering its multiple isomers and conformers, and the solvent-dependence of its properties. Based on the geometry optimizations by DFT, the molecule **1** as prepared by the synthesis, without any light irradiation, is in the *E* form, with two different possible conformers, namely *s-trans*-(*E*)-**1** and *s-cis*-(*E*)-**1**. The most stable conformer is the *s-trans*-(*E*)-**1**, as shown by the XRD structure

and the relative energies between the two E geometries (ΔE=1.9 kcal mol^{-1} by DFT in vacuum). Both conformers are expected to be populated at room temperature with a Boltzmann distribution of ~96:4 (*s-trans*-(*E*)-**1**/*s-cis*-(*E*)-**1**), but cannot be easily distinguished by steady-state spectroscopy, due to fast conformational interconversion and the likely overlap of their respective spectral contributions. The main absorption and emission spectral features are nevertheless attributed to the *s-trans*-(*E*)-**1** isomer: the large emission Stokes shifts recorded at higher solvent polarity are consistent with previous studies on DCM,[3b, 9] due to extended π-conjugation and intramolecular charge-transfer character between the aniline electron-donating group and the dicyanomethylene-pyranyl electron-withdrawing group, with planar geometry and large dipole moment in the ground state, which is dramatically enhanced in the excited state ($\Delta\mu$=14.4 D).[9a] Time-resolved spectroscopy is a powerful tool to resolve conformational mixtures, identify the number of species and their respective lifetimes. Fluorescence decays of (*E*)-**1** before irradiation highlighted two decay-time components τ_1 (largest contribution) and τ_2 (minor weight). The major component τ_1 has been naturally assigned to the lifetime of the most stable form *s-trans*-(*E*)-**1**, while the second component τ_2 could be ascribable to the presence of a very small fraction of *s-cis*-(*E*)-**1** isomer. The recorded values for τ_1 are in accordance with previous time-resolved studies on DCM.[13b, 13c] The contribution of *s-cis*-(*E*)-**1** to the overall fluorescence is limited to few percent (f_2 <0.03) due to its limited population and short lifetime (τ_2 <0.43 ns), slightly blue-shifted with respect to the main *s-trans*-(*E*)-**1** conformer (f_2 is larger at shorter wavelengths, Table 2). Considering the emission quantum yield (Φ_{em}), the lifetime related to the main *s-trans*-(*E*)-**1** isomer (τ_1) and its contribution (f_1), the radiative (k_r) and nonradiative (k_{nr}) deactivation rate constants can be determined as follows [Eqs. 6 and 7]:

$$k_r = \frac{f_1 \times \Phi_{em}}{\tau_1}$$

(6)

$$k_{nr} = \frac{1 - f_1 \times \Phi_{em}}{\tau_1}$$

(7)

The magnitude of the radiative rate constant k_r is calculated to be almost unchanged in the three solvents (1.4–2.5×10^8 s^{-1}), meaning that the electronic nature of the *s-trans*-(*E*)-**1** emissive state does not critically depend on the solvent polarity. Conversely, the nonradiative deactivation rate constant k_{nr} increases dramatically from polar to nonpolar solvents, namely from 2.0×10^8 s^{-1} in MeCN to 7.0×10^9 s^{-1} in PhMe. This effect can be attributed both to the intrinsic vibrational relaxation of the excited state and the solvent-dependent $E \rightarrow Z$ photoreactivity, which is enhanced by a factor two in PhMe compared to MeCN and THF (vide infra). In principle, a comparable determination of k_r and k_{nr} could be made for the *s-cis*-(*E*)-**1** isomer, Equations (6) and (7) being derived with f_2 and τ_2: the radiative rate is approximately 10 times smaller for *s-cis*-(*E*)-**1** than *s-trans*-(*E*)-**1**, and the nonradiative rate is approximately 10 times higher. Such parameters are likely due to the different conjugation geometry and lower stability of this conformer. However, the accuracy on the k_r and k_{nr} values of *s-cis*-(*E*)-**1** must be considered with caution, given the relatively large uncertainty on this minor component in time-resolved measurements.

The (*Z*)-**1** isomer is generated by light irradiation, as demonstrated by steady-state absorption spectral changes under illumination. However, this isomer has been found to be non-fluorescent, as indicated by: 1) the absence of variation in the decay times and pre-exponential factors before and after irradiation (Table 2), 2) the extrapolation to zero emission signal at total $E \rightarrow Z$ conversion (Figure 6 c), and 3) the absence of change in the excitation spectrum when (*E*)-**1** is irradiated (Figure 6 c, inset). These experimental evidences suggest that the recorded emission is solely ascribable to the E isomer, namely the *s-trans*-(*E*)-**1** and *s-cis*-(*E*)-**1** conformers, as discussed in the

previous paragraph. The (*Z*)-**1** form may also exist in the two conformers *s-cis*-(*Z*)-**1** and *s-trans*-(*Z*)-**1**: they easily interconvert at room temperature ($\Delta E \sim 1.2$ kcal mol^{-1}, according to DFT calculations in vacuum) and cannot be properly identified. The overall proportions of (*E*)-**1** versus (*Z*)-**1** isomers can then be considered in the following, summing the contributions of the *s-trans* and *s-cis* conformers.

Although largely ignored in the literature, where the DCM derivatives are widely employed as simple fluorophores, the $E{\rightarrow}Z$ and $Z{\rightarrow}E$ photoisomerization reactions of **1** occur with high efficiencies. The quantum yields Φ_{EZ} and Φ_{ZE}, as well as the conversion yield α_Z, strongly depend on the irradiation wavelength chosen to trigger the photoswitching. The $E{\rightarrow}Z$ photoconversion is favored at 485 and 514 nm, whereas the $Z{\rightarrow}E$ reaction can be induced at 365 nm. The thermal back-reaction is very slow, the switching rates are fast and the fatigue resistance is quite satisfying, without noticeable degradation after 15 visible–UV switching cycles. Therefore, the compound **1** can be considered as an efficient bi-stable P-type photochromic derivative,[19] with quite promising fluorescence photoswitchability between the fluorescent (*E*)-**1** form and the non-fluorescent (*Z*)-**1** isomer. The subtle fluorescence versus photoisomerization balance is depicted in Figure 9, gathering the main photophysical parameters related to fluorescence (fluorescence quantum yield Φ_{em} and averaged lifetime $\langle\tau\rangle$, Figure 9 a) and photoisomerization properties ($E{\rightarrow}Z$ and $Z{\rightarrow}E$ photoreaction quantum yields, conversion yield α_Z at the PSS 485 nm, Figure 9 b) in MeCN, THF and PhMe. The solvent has a dramatic effect on the observed properties. In MeCN, the compound **1** appears to hold excellent fluorescence properties (bright emission, long decay-time) but rather poor photoisomerization capability (limited $E{\rightarrow}Z$ quantum yield and conversion extent). In PhMe, the E–Z isomerization is greatly improved (higher Φ_{EZ}, Φ_{ZE} and α_Z) but the fluorescence is very weak. Interestingly, THF appears as an ideal trade-off between fluorescence and photoisomerization properties, with a significant fluorescence quantum yield of the (*E*)-**1** isomer and a large $E{\rightarrow}Z$ photoconversion under visible irradiation (α_Z=0.46 at 485 nm, where absorption is large), due to higher Φ_{EZ} and lower Φ_{ZE} quantum yields compared to other solvents. Therefore, the compound **1** in THF represents an excellent candidate in terms of fluorescence photoswitching (Figure 9).
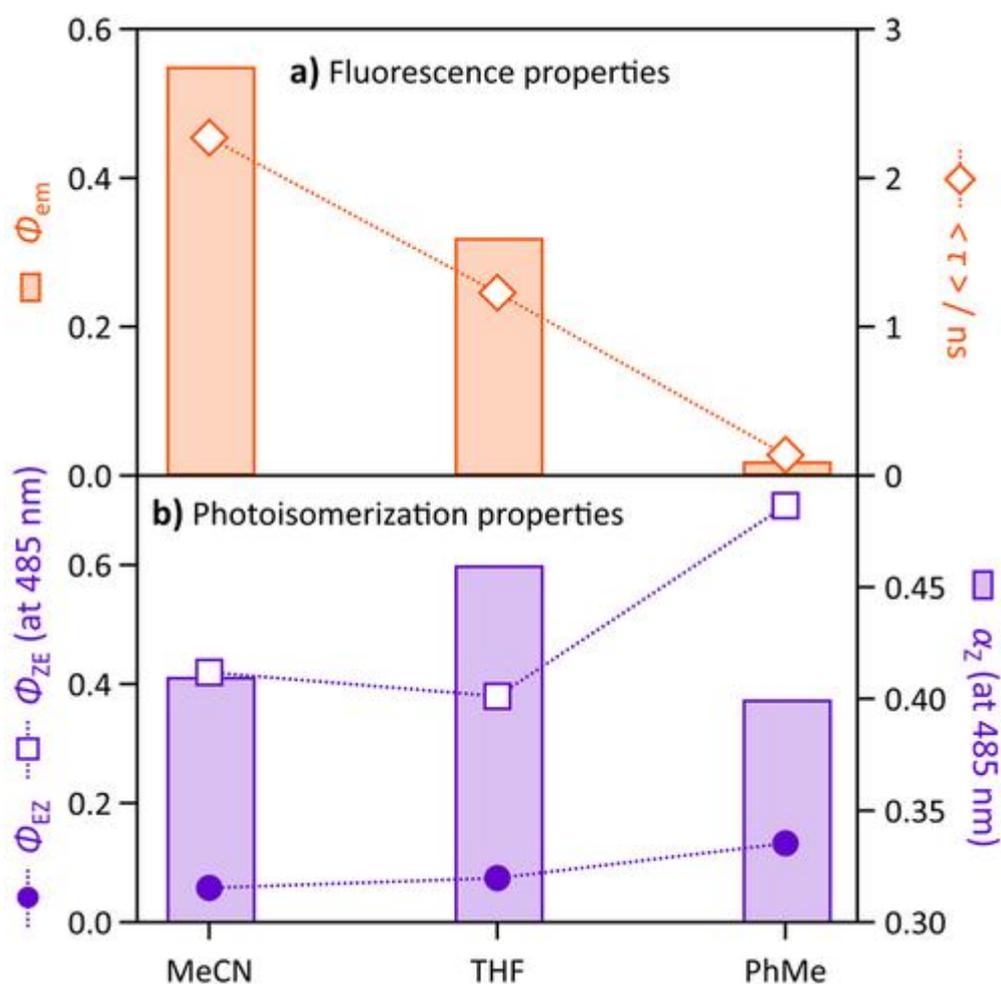
Figure 9. Summary of the photophysical and photochemical properties of **1** as a function of the solvent. a) Fluorescence parameters (emission quantum yield Φ_{em}, averaged lifetime $\langle\tau\rangle$) and b) photoisomerization parameters ($E{\rightarrow}Z$ and $Z{\rightarrow}E$ quantum yields Φ_{EZ} and Φ_{ZE}, respectively, and conversion yield α_Z at the PSS 485 nm). $\langle\tau\rangle$ is defined as $\Sigma f_i{\times}\tau_i$.

Conclusions

In conclusion, we have characterized the fluorescence and photoisomerization properties of the DCM-based derivative **1**. The fluorescence of the initial (E)-**1** isomer turned out to be strongly sensitive to the solvent, in terms of emission wavelength, quantum yield and decay time. These environment-sensitive features are very attractive for a large variety of applications of this family of fluorophores (DCM derivatives) as sensors. The (E)-**1** isomer exists mostly in its *s-trans*-(E)-**1** form, as determined by single crystal XRD, but also in a small fraction of *s-cis*-(E)-**1**, as demonstrated by time-resolved spectroscopy and theoretical calculations. Beyond these expected fluorescence properties, compound **1** undergoes E–Z photoisomerization under visible and UV irradiation. This property has been qualitatively mentioned in several reports,[10a, 11b, 13] but ignored in the vast majority of related papers in the field. The (E)-**1** and (Z)-**1** isomers have been indeed quantified by HPLC, thus allowing the precise determination of α_Z conversion yield, which represents the fraction of (Z)-**1** form at the PSS. We demonstrated that the (Z)-**1** isomer is not

emissive or thermally stable in typical experimental timescales. The detailed investigation of the photoisomerization quantum yields Φ_{EZ} and Φ_{ZE} of the compound **1** highlights the great sensitivity of its $E{\rightarrow}Z$ and $Z{\rightarrow}E$ photoreactions to solvent polarity and irradiation wavelength. The light-induced transitions between PSS of different Z/E compositions are achieved at multiple irradiation wavelengths (in the visible and in the UV) with fast rates and excellent fatigue resistance. It is interesting to highlight that experimental conditions can be chosen in order to maximize both fluorescence and photochromic properties of **1**, and enhance the amplitude of the fluorescence photoswitching. Considering the wide range of applications involving the DCM fluorophore, such an insight to the photochemical and photophysical properties of **1** is expected to open important horizons in terms of photoresponsive molecular probes and materials. Compound **1** can be indeed considered as an efficient fluorescent-photochromic dye, and the terminal alkynyl group can be advantageously employed to incorporate **1** into target molecular materials (proteins, supramolecular systems) by copper-catalyzed Huisgen 1,3-dipolar cycloaddition reaction. Such photoresponsive fluorophores could find promising new perspectives[20] for the design of multistate molecular systems entailing optimized photoswitchable fluorescence.

Experimental Section

Crystallographic analysis

X-ray crystallographic analysis were conducted on samples obtained by recrystallization: 7.13 g of compound **1** were dissolved in 125 mL of CH_3CN, heated to 85 °C over 30 min, then cooled to room temperature and the solid filtered off to give dark red crystals. The isolated crystals were dried under vacuum at room temperature (m.p.: 156 °C). X-ray experiment was carried out at the $Cu_{K\alpha}$ wavelength on a Rigaku mm007HF diffractometer constituted by a MicroMax™-007 microfocus rotating anode with Osmic CMF optics and a curved rapid2 IP detector and at ambient temperature. Computing details: data collection/cell refinement/data reduction: CrystalClear-SM expert 2.0 (Rigaku, 2009); program(s) used to solve structure: Shelxt (Sheldrick, 2015); program(s) used to refine structure: Shelxl-2014/7 (Sheldrick, 2015); molecular graphics: PLATON (Spek, 2009); software used to prepare material for publication: Shelxl-2014/7 (Sheldrick, 2015).

Separation methods

High-performance liquid chromatography (HPLC) analyses were performed on previously irradiated solutions, with an analytical HPLC chain from Shimadzu, model Prominence UFLC equipped with two LC-20AD pumping modules, a CTO-20AC oven, a thermostatically controlled SPD-M20A module, a thermostatic photodiode array (190–800 nm, 40 °C, slits 4 nm) for UV/Vis absorption detection, and a CBM-20A communication module. The injection was carried out using a 5 µL injection loop and a Rheodyne 7725i valve. The separation was carried out at 40 °C using a core–shell C_{18} grafted silica chromatographic column, model Phenomenex Kinetex Evo-C18 column (particle size 5 µm, pores size 100 Å, length 250 mm, internal diameter 4.6 mm) and equipped with a pre-filter. Data were acquired with the LabSolutions V 5.71 SP2 software from Shimadzu Corporation. The purchased solvents from Carlo–Erba Reagents (Dasit group) with a spectroscopic or HPLC grade were degassed under sonication.

Steady-state absorption and emission spectroscopy

Steady-state spectroscopic measurements were performed in spectroscopic grade solvents (Carlo Erba Reagents, Dasit group) solutions at room temperature. Quartz cuvettes with a 1 cm path length were used. UV/vis absorption spectra were recorded with Agilent Technologies Cary 100, Cary 4000, and Cary 5000 spectrophotometers. Emission and excitation spectra were recorded on a Horiba Jobin–Yvon Fluorolog FL3-221 or Fluoro-Max3 fluorescence spectrometers. Emission quantum yields were determined using Coumarine 153 in ethanol (Φ_{em}=0.544)[21] as a standard for **1** in all the three solvents.

Time-resolved fluorescence spectroscopy

Fluorescence decays were measured by the time-correlated single-photon counting (TCSPC) technique. A femtosecond laser excitation was performed by a titanium/sapphire laser (Tsunami, Spectra-Physics) pumped by a doubled Nd:YVO4 laser (Millennia Xs from Spectra-Physics). Light pulses at 800 nm from the oscillator were selected by an acousto-optic crystal at a repetition rate of 4 MHz, and then doubled at 400 nm by nonlinear crystals. Fluorescence photons were detected at 90°, through a polarizer at the magic angle, by means of a Hamamatsu MCP R3809U photomultiplier, connected to a SPC-630 TCSPC module from Becker & Hickl. The instrumental response function was recorded before each decay measurement with a FWHM (full width at half-maximum) of 23 ps. The fluorescence data were analyzed using the Globals software package developed by the Laboratory for Fluorescence Dynamics at the University of California, Irvine, which includes reconvolution analysis and the global nonlinear least-squares minimization method.

Photoisomerization studies

Irradiation experiments were performed at room temperature, on vacuum-deoxygenated solutions. Hamamatsu Hg-Xe lamps LC8 or LC6–Lightningcure (200 W) were employed as excitation source. The desired wavelengths were selected using appropriate Semrock or Oriel interferential filters, listed in Table S2. The incident lamp power was measured by means of an Ophir PD300-UV photodiode. NIR contribution has been measured and subtracted from the total value. Photoisomerization quantum yields and fatigue resistances were determined using a home-made setup, that allows to collect absorption spectra with high rates, under continuous irradiation. A Xenon lamp (75 W) was used as a probing light source, and a Hg/Xe lamp, placed at 90° with respect to the incident beam, was used to induce the photochromic reaction in the sample, placed in a cuvette and thoroughly stirred. Spectra were recorded every 0.2 s, with a spectrometer coupled with a CCD (Roper Scientific and Princeton Instruments, respectively).

Computational methods

Geometry optimization was performed using the PBE0 exchange functional. The basis set 6–311G+(d,p) has been chosen, implemented in the Gaussian09 software package.[22] The absence of negative frequencies was checked to ensure true minima for all geometries.

Acknowledgements

Conflict of interest

The authors declare no conflict of interest.

References

1a. V. Balzani, A. Credi, M. Venturi, Molecular Devices and Machines: A Journey into the Nano World, Wiley-VCH, Weinheim, 2003;

1b. B. L. Feringa, W. R. Brown, Molecular Switches , 2nd ed., Wiley-VCH, Weinheim, 2011;

1c. H. Dong, H. Zhu, Q. Meng, X. Gong, W. Hu, *Chem. Soc. Rev.* 2012, 41, 1754– 1808;

1d. Z. Tian, A. D. Li, *Acc. Chem. Res.* 2013, 46, 269– 279;

1e. M. E. Gemayel, K. Borjesson, M. Herder, D. T. Duong, J. A. Hutchison, C. Ruzie, G. Schweicher, A. Salleo, Y. Geerts, S. Hecht, E. Orgiu, P. Samori, *Nat. Commun.* 2015, 6, 6330;

1f. Photochromic Materials: Preparation, Properties and Applications (Eds.: H. Tian, J. Zhang), Wiley-VCH, Weinheim, 2016.

2. P. R. Hammond, *Opt. Commun.* 1979, 29, 331– 333.

3a. E. G. Marason, *Opt. Commun.* 1981, 37, 56– 58;

3b. J.-C. Mialocq, M. Meyer, *Laser Chem.* 1990, 10, 277– 296.

4a. J. Bourson, B. Valeur, *J. Phys. Chem.* 1989, 93, 3871– 3876;

4b. Y. Suzuki, K. Yokoyama, *J. Am. Chem. Soc.* 2005, 127, 17799– 17802;

4c. W. Zhu, X. Huang, Z. Guo, X. Wu, H. Yu, H. Tian, *Chem. Commun.* 2012, 48, 1784– 1786;

4d. Y. Zheng, M. Zhao, Q. Qiao, H. Liu, H. Lang, Z. Xu, *Dyes Pigm.* 2013, 98, 367– 371;

4e. X. Wu, X. Sun, Z. Guo, J. Tang, Y. Shen, T. D. James, H. Tian, W. Zhu, *J. Am. Chem. Soc.* 2014, 136, 3579– 3588;

4f. S. Chen, Y. Fang, Q. Zhu, W. Zhang, X. Zhang, W. Lu, *RSC Adv.* 2016, 6, 81894– 81901.

5a. C. Ma, B. Zhang, Z. Liang, P. Xie, X. Wang, B. Zhang, Y. Cao, X. Jiang, Z. Zhang, *J. Mater. Chem.* 2002, 12, 1671– 1675;

5b. Q. Peng, Z.-Y. Lu, Y. Huang, M.-G. Xie, S.-H. Han, J.-B. Peng, Y. Cao, *Macromolecules* 2004, 37, 260– 266;

5c. M. K. Leung, C. C. Chang, M. H. Wu, K. H. Chuang, J. H. Lee, S. J. Shieh, S. C. Lin, C. F. Chiu, *Org. Lett.* 2006, 8, 2623– 2626;

5d. Y. S. Yao, J. Xiao, X. S. Wang, Z. B. Deng, B. W. Zhang, *Adv. Func. Mater.* 2006, 16, 709– 718.

6a. W. Ballet, I. Picard, T. Verbiest, A. Persoons, C. Samyn, *Macromol. Chem. Phys.* 2004, 205, 13– 18;

6b. R. Andreu, L. Carrasquer, J. Garín, M. J. Modrego, J. Orduna, R. Alicante, B. Villacampa, M. Allain, *Tetrahedron Lett.* 2009, 50, 2920– 2924.

7a. L. Jullien, J. Canceill, B. Valeur, E. Bardez, J.-P. Lefèvre, J.-M. Lehn, V. Marchi-Artzner, R. Pansu, *J. Am. Chem. Soc.* 1996, 118, 5432– 5442;

7b. K. Ouhenia-Ouadahi, R. Métivier, S. Maisonneuve, A. Jacquart, J. Xie, A. Leaustic, P. Yu, K. Nakatani, *Photochem. Photobiol. Sci.* 2012, 11, 1705– 1714;

7c. S. Maisonneuve, R. Métivier, P. Yu, K. Nakatani, J. Xie, *Beilstein J. Org. Chem.* 2014, 10, 1471– 1481.

8a. Z. Guo, W. Zhu, L. Shen, H. Tian, *Angew. Chem. Int. Ed.* 2007, 46, 5549– 5553; *Angew. Chem.* 2007, 119, 5645– 5649;

8b. Z. Guo, P. Zhao, W. Zhu, X. Huang, Y. Xie, H. Tian, *J. Phys. Chem. C* 2008, 112, 7047– 7053;

8c. Z. Guo, W. Zhu, Y. Xiong, H. Tian, *Macromolecules* 2009, 42, 1448– 1453;

8d. Z. Guo, W. Zhu, H. Tian, *Chem. Commun.* 2012, 48, 6073– 6084.

9a. M. Meyer, J. C. Mialocq, *Opt. Commun.* 1987, 64, 264– 268;

9b. R. Lapouyade, A. Kuhn, J.-F. Letard, W. Rettig, *Chem. Phys. Lett.* 1993, 208, 48– 58.

10a. M. Meyer, J. C. Mialocq, B. Perly, *J. Phys. Chem.* 1990, 94, 98– 104;

10b. H. Zhang, A. M. Jonkman, P. van der Meulen, M. Glasbeek, *Chem. Phys. Lett.* 1994, 224, 551– 556;

10c. M. M. Martin, P. Plaza, Y. H. Meyer, *Chem. Phys.* 1995, 192, 367– 377;

10d. S. Pommeret, T. Gustavsson, R. Naskrecki, G. Baldacchino, J.-C. Mialocq, *J. Mol. Liq.* 1995, 64, 101– 112;

10e. A. Maciejewski, R. Naskrecki, M. Lorenc, M. Ziolek, J. Karolczak, J. Kubicki, M. Matysiak, M. Szymanski, *J. Mol. Struct.* 2000, 555, 1– 13;

10f. A. J. Van Tassle, M. A. Prantil, G. R. Fleming, *J. Phys. Chem. B* 2006, 110, 18989– 18995.

11a. M. Sun, T. Pullerits, P. Kjellberg, W. J. D. Beenken, K. Han, *J. Phys. Chem. A* 2006, 110, 6324– 6328;

11b. X. Xu, R. Zhang, Z. Cao, Q. Zhang, *J. Theor. Comput. Chem.* 2008, 07, 719– 736;

11c. I. D. Petsalakis, D. G. Georgiadou, M. Vasilopoulou, G. Pistolis, D. Dimotikali, P. Argitis, G. Theodorakopoulos, *J. Phys. Chem. A* 2010, 114, 5580– 5587.

12a. S. K. Pal, D. Mandal, D. Sukul, K. Bhattacharyya, *Chem. Phys. Lett.* 1999, 312, 178– 184;

12b. S. K. Pal, D. Sukul, D. Mandal, K. Bhattacharyya, *J. Phys. Chem. B* 2000, 104, 4529– 4531;

12c. D. Mandal, S. Sen, K. Bhattacharyya, T. Tahara, *Chem. Phys. Lett.* 2002, 359, 77– 82;

12d. A. Halder, P. Sen, A. D. Burman, K. Bhattacharyya, *Langmuir* 2004, 20, 653– 657.

13a. M. Lesiecki, F. Asmar, J. M. Drake, D. M. Camaioni, *J. Lumin.* 1984, 31, 546– 548;

13b. J. M. Drake, M. L. Lesiecki, D. M. Camaioni, *Chem. Phys. Lett.* 1985, 113, 530– 534;

13c. M. Meyer, J. C. Mialocq, M. Rougée, *Chem. Phys. Lett.* 1988, 150, 484– 490;

13d. W. Rettig, W. Majenz, *Chem. Phys. Lett.* 1989, 154, 335– 341;

13e. J. C. Mialocq, X. Armand, S. Marguet, *J. Photochem. Photobiol. A* 1993, 69, 351– 356.

14. C. De Schutter, V. Roy, P. Favetta, C. Pavageau, S. Maisonneuve, N. Bogliotti, J. Xie, L. A. Agrofoglio, *Org. Biomol. Chem.* 2018, 16, 6552– 6563.

15. D. J. S. Birch, G. Hungerford, R. E. Imhof, A. S. Holmes, *Chem. Phys. Lett.* 1991, 178, 177– 184.

16. K. Nakatani, J. Piard, P. Yu, R. Métivier in Photochromic Materials: Preparation, Properties and Applications, 1st ed. (Eds.: H. Tian, J. Zhang), Wiley-VCH, Weinheim, 2016, pp. 1– 45.

17. D. H. Waldeck, *Chem. Rev.* 1991, 91, 415– 436.

18a. H. M. Bandara, S. C. Burdette, *Chem. Soc. Rev.* 2012, 41, 1809– 1825;

18b. C. Knie, M. Utecht, F. Zhao, H. Kulla, S. Kovalenko, A. M. Brouwer, P. Saalfrank, S. Hecht, D. Bleger, *Chem. Eur. J.* 2014, 20, 16492– 16501.

19a. F. M. Raymo, *J. Phys. Chem. Lett.* 2012, 3, 2379– 2385;

19b T. Fukaminato, S. Ishida, R. Métivier, *NPG Asia Mater.* 2018, 10, 859– 881.

20 B. Shao, M. Baroncini, H. Qian, L. Bussotti, M. Di Donato, A. Credi, I. Aprahamian, *J. Am. Chem. Soc.* 2018, 140, 12323– 12327.

21. K. Rurack, M. Spieles, *Anal. Chem.* 2011, 83, 1232– 1242.

22. Gaussian 09, Revision A.02, M. J. Frisch, G. W. Trucks, H. B. Schlegel, G.E. Scuseria, M. A. Robb, J.R. Cheeseman, G. Scalmani, V. Barone, G.A. Petersson, H. Nakatsuji, X. Li, M. Caricato, A. Marenich, J. Bloino, B.G. Janesko, R. Lipparini, F. Egidi, J. Goings, B. Peng, A. Petrone, T. Henderson, D. Ranasinghe, V. G. Zakrzewski, J. Gao, N. Rega, G. Zheng, W. Liang, M. Hada, M. Ehara, K. Toyota, R. Fukuda, J.

Hasegawa, M. Ishida, T. Nakajima, Y. Honda, O. Kitao, H. Nakai, T. Vreven, K. Throssell, J.A. Montgomery, J.E. Peralta, F. Ogliaro, M. Bearpark, J.J. Heyd, E. Brothers, K. N. Kudin, V. N. Staroverov, T. Keith, R. Kobayashi, J. Normand, K. Raghavachari, A. Rendelll, J. C. Burant, S. S. Iyengar, J. Tomasi, M. Cossi, J. M. Millam, M. Klene, C. Adamo, R. Cammi, J. W. Ochterski, R.L. Martin, K. Morokuma, O. Farkas, J. B. Foresman, D. J. Fox, Gaussian, Inc., Wallington CT, **2016**.